

1 **Electrochemically deposited zinc oxide films on stainless steel for photo**
2 **degradation of Basic Red 18 dye**

3
4 Doğan Cirmi¹, Zeynep Bilici², Nadir Dizge², M. Shameer Basha³, B. Deepanraj^{4*}, Jasgurpreet
5 Singh Chohan⁵

6
7 ¹ *Department of Chemistry, Mersin University, Mersin, 33343, Turkey*

8 ² *Department of Environmental Engineering, Mersin University, Mersin, 33343, Turkey*

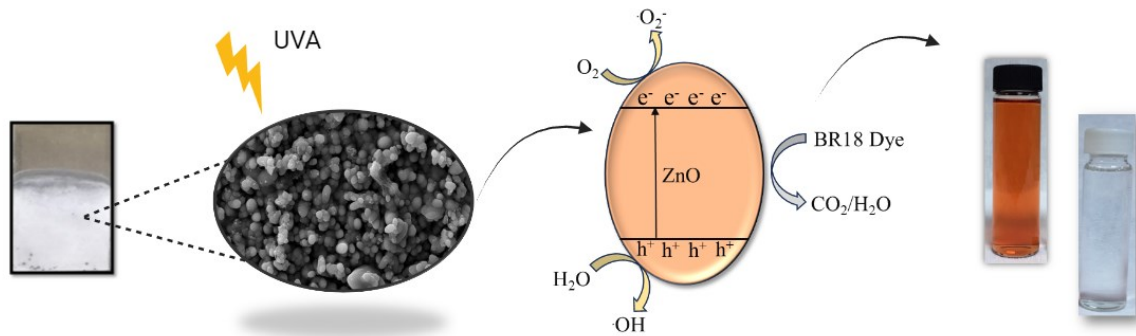
9 ³ *Department of Mechanical Engineering, College of Engineering, Qassim University,*
10 *Buraidah-51452, Saudi Arabia.*

11 ⁴ *Department of Mechanical Engineering, Prince Mohammad Bin Fahd University,*
12 *Al-Khobar, 31952, Saudi Arabia*

13 ⁵ *University Centre for Research & Development, Department of Mechanical Engineering,*
14 *Chandigarh University, Gharuan, Punjab, India*

15
16
17
18 * Corresponding author email: babudeepan@gmail.com

27 **Graphical Abstract**



28

29 **Abstract**

30 In this study, zinc oxide (ZnO) films have been electrochemically deposited on stainless steel
31 and its photocatalytic activity on the degradation of BR 18 dyes was tested. The effects of
32 different electrodeposition conditions such as deposition potential and deposition time on the
33 nanostructures of ZnO films were investigated in detail and the best electrodeposition
34 conditions were optimized. The electrochemical, structural and morphological, were
35 characterized by cyclic voltammetry (CV), chronoamperometry, X-ray diffraction (XRD),
36 scanning electron microscope (SEM), respectively. The best removal efficiency was 37% at -
37 1.2 V, and increased up to 53% after 300 sec coating. The number of electrodes (1, 2, 3 and 4
38 coatings) and dye concentration (5, 10, 15 mg/L) covered with -1.2 V potential and the coating
39 synthesized in 300 seconds were studied. A complete removal was obtained when the number
40 of electrodes covered was 4 and at 5 mg/L initial dye concentration. The number of reuses was
41 tested up to 5 cycles. ZnO coatings on stainless steel that were electrochemically charged
42 showed good photocatalytic stability. Because ZnO films have both economic and
43 environmental advantages, it is imperative that they can be synthesized using environmentally
44 benign processes and used in photocatalysis. This novel strategy provides a chance to utilize
45 ZnO film photocatalytic characteristics for a range of environmental remediation applications
46 in addition to providing a sustainable wastewater management solution.

47

48

49 *Keywords: Electrodeposition, ZnO, Photocatalytic oxidation, BR18 dye*

50

51

52
53
54
55
56
57
58
59
60
61 **1. Introduction**

62 Water pollution is the water that is formed as a result of the use of water resources as a result
63 of industrial, agricultural, and domestic activities and has lost its natural characteristics
64 (Tarazona 2014, Lamkhao et. al. 2023). Water pollution, which is an important environmental
65 problem throughout the world, greatly affects the lives of living things (Earnhart 2013).
66 Wastewater from industrial activities (chemistry, metals, petroleum, leather, textiles, food, etc.)
67 creates wastewater with a high pollution load. When these wastewaters are given to the
68 receiving environment (rivers, lakes, seas, groundwater, etc.) without treatment, they pose
69 serious threats to human health and disrupt the ecosystem balance (Antoniadis et al.
70 2007). Wastewater from the textile industry causes serious pollution due to the loss of 15-20%
71 of the dyes consumed during the process (Ghalebizade and Ayati 2016). Azo dyes are common
72 and important compounds in the textile industry that contain N=N chemical bonds. Wastewater
73 with a high concentration of dyes originating from this industry needs to be treated because it
74 is harmful to the environment, carcinogenic, and toxic (Roy et al. 2020). The textile industry
75 frequently uses water-soluble synthetic dyes like Basic Red 18 (BR 18), which is a cationic dye
76 (Ugur et al., 2021). BR 18, which is an azo dye, can destroy the aquatic environment's biological
77 activity, produce color pollution, and reduce clarity. Moreover, synthetic azo dyes provide a
78 significant risk to human health due to all of these factors, requiring their rapid removal from
79 aquatic environments (Mahmoodi et. al. 2016).

80 The treatment of textile wastewater is difficult due to high flow rates and pollution (Hasanbeigi
81 and Price 2015). Coagulation, adsorption, membrane filtration, electrocoagulation, Fenton,
82 photo-electro Fenton and photocatalytic systems are widely used in the treatment of textile
83 wastewater (Tao and Wang 2023). Biological treatment is not used alone, as it is insufficient for

84 the decomposition of dangerous aromatic compounds. Cost-intensive physical techniques
85 include membrane filtration, coagulation, adsorption, and electrocoagulation (Naseri et al.
86 2021). Advanced oxidation processes are used to provide wastewater treatment by breaking
87 down synthetic azo dyestuffs. These processes produce hydroxyl radicals, which degrade
88 organic compounds and other pollutants (Naseri et al. 2021). Photocatalytic oxidation, one of
89 the advanced oxidation processes, is wastewater treatment using a catalyst under sunlight or
90 UV light (Bethi et al. 2016).

91 BR 18 dye was removed from aqueous solution using basalt powder as a heterogeneous catalyst
92 for the Fenton and photo-Fenton reactions. The removal efficiencies for BR 18 by the Fenton
93 and photo-Fenton process were 87% and 70%, respectively, at 70 mg/L dye concentration, 5
94 mM H₂O₂ concentration, 1.0 g/L basalt amount and pH 2 (Saleh et al. 2021). In another study,
95 ZnO/MoS₂/rGO composite catalyst was used for photocatalytic decolorization of BR 18 dye.
96 The results showed that 100% removal efficiency was achieved for 25ZnO/75MG2 at 25 mg/L
97 initial dye concentration and 0.5 g/L catalyst amount for 60 min (Ugur et al. 2021). Eskikaya et
98 al. (2022) investigated photocatalytic activity of zinc oxide nanoflowers (ZnO-NFs) for BR 18
99 removal from aqueous solution. ZnO-NFs were synthesized by two different processes
100 hydrothermal method (named ZnO-NF1) and the precipitation method (named ZnO-NF2). BR
101 18 was completely removed at 25 mg/L BR18 dye concentration using 1.5 g/L ZnO-NF1
102 amount for 75 min.

103 Zinc oxide (ZnO) is a compound used as an important photocatalyst due to both its
104 photocatalytic properties and its inexpensive, environmentally friendly and non-toxicity
105 (Kohzadi et al. 2023). Many methods have been developed to prepare ZnO thin films such as
106 chemical vapor deposition, sol gel, pulsed laser deposition, hydrothermal methods and
107 electrochemical methods (Rekha et al. 2023). Electrochemical method has many advantages
108 such as the mass, thickness, morphology, low-temperature processing, low cost process and
109 good electrical contact between structures and substrate.

110 When ZnO is excited under sunlight, the electrons on its surface rise to higher energy levels,
111 causing the formation of free radicals such as reactive oxygen species hydroxyl radicals (OH•)
112 and superoxide radicals (O₂•-) (Kumar et al. 2021, Elshahawy et al. 2023). These free radicals
113 break down organic pollutants and other harmful substances, provides them to be cleaned
114 (Elshahawy et al. 2023). ZnO photocatalysis stands out as an environmentally friendly,
115 sustainable purification and cleaning method (Selvaraj et al. 2022). Helping to neutralize
116 pollutants by using a clean and renewable energy source such as sunlight contributes to reducing

117 environmental pollution and protecting the environment (Singh, 2022). It is also used in areas
118 such as water treatment, air cleaning, self-cleaning surfaces, energy generation (Fiorenza et al.
119 2023).

120 In this study, we prepared electrochemical technique of deposition ZnO film on a Stainless
121 Steel. The effects of deposition parameters, such as the deposition time and applied potential
122 were also investigated. It was aimed to examine the effect of ZnO on the coating under different
123 conditions and to increase its reuse without loss of catalyst. In addition to examining the
124 decomposition products of BR18 using a photocatalytic system, the effect of ZnO on parameters
125 such as voltage change, H₂O₂ concentration, contact time during plating on stainless steel was
126 studied. Kinetic, dye concentration and reuse experiments were carried out with the coating
127 obtained under optimum conditions.

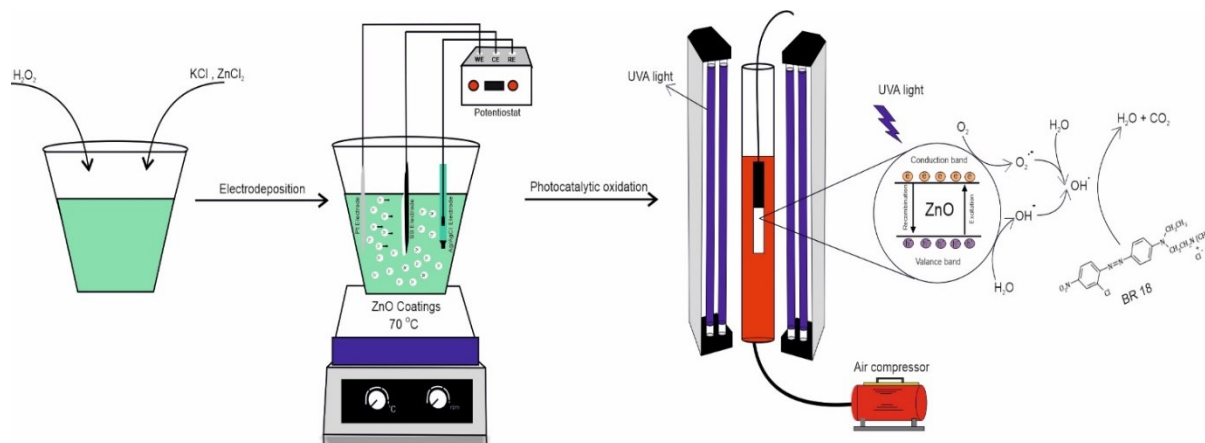
128 **2. Material and Methods**

129 *2.1. Materials*

130 All chemicals used in this work without further purification were of analytical grade. The
131 substrate is Stainless Steel (SS) type 316 cut with dimensions 1 cm × 2 cm. Zinc chloride
132 (ZnCl₂, Merck, Germany), Potassium chloride (KCl, Merck, Germany) and Hydrogen peroxide
133 (H₂O₂, Merck, Germany) were used. BR18 azo dyestuff was prepared as 100 mg/L stock
134 solution in distilled water.

135 *2.2. Electrochemical synthesis of ZnO*

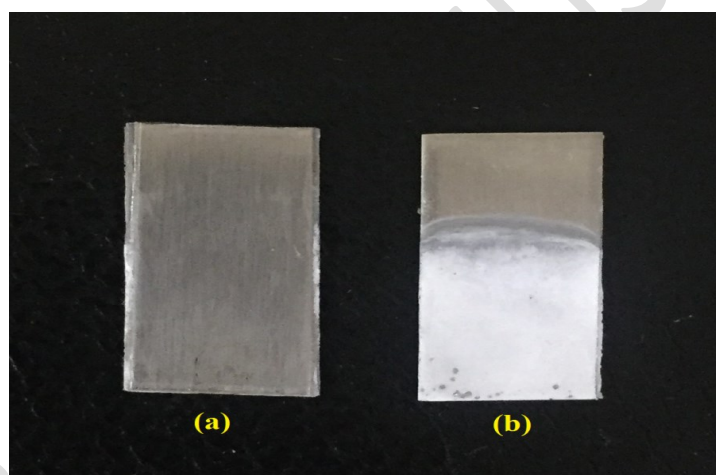
136 The electrodeposition of ZnO thin films were carried out using a potentiostat/galvanostat (CHI
137 660C, CH Instruments). The 316 stainless steel (SS) (1 cm × 2 cm), a Ag/AgCl (saturated KCl)
138 and a platinum plate (1 cm × 2 cm) has been used as working electrode, reference electrode and
139 counter electrode, respectively (Fig. 1). Prior to electrodeposition, the SS substrates were
140 ultrasound cleaned with acetone and distilled water. An aqueous solution of 0.05 M ZnCl₂, 0.1
141 M KCl and 20 mM H₂O₂ was used as electrolyte. The temperature was maintained at 70 °C
142 throughout the deposition process. ZnO nanoparticles were distributed uniformly through
143 electrodeposition process optimization. Investigated were the effects of electrodeposition times
144 (120, 180, 300, and 420 s) and potentials (from -1.1 V, -1.2 V, and -1.3 V vs. Ag/AgCl).



145

146 **Fig. 1.** A schematic representation of the experimental set up

147 A photograph belongs to stainless steel coated with ZnO is shown in Fig. 2.



148

149 **Fig 2. (a)** Stainless steel, **(b)** ZnO-coated stainless steel

150 2.3. Characterization techniques

151 ZnO film electrodeposition was performed with a potentiostat/galvanostat (CHI 660A, CH
 152 Instruments, U.S.A.). The morphology, particle size, and elemental composition of the
 153 electrodes were examined using a scanning electron microscope (model Quanta 650) fitted with
 154 an EDX detector. The X-ray diffraction spectra (XRD) analysis was performed using Cu-K α (λ
 155 = 1.54 Å) irradiation as an X-ray source (40 kV/30 mA) and Empyrean (PANalytical) operating
 156 in a 2θ scan from 30° to 80°.

157 2.4. Photocatalytic studies

158 In this study, ZnO coating was applied on stainless steel (1cm × 2 cm) and its photocatalytic
159 effect on BR18 dye removal was investigated. The system was carried out using 6 UVA lamps
160 (Philips TL8W Actinic BL) at 365 nm wavelength in a circular reactor covered with aluminum
161 foil. The luminous intensity and wavelength of the lamps used are 3.5 mW/cm² and 365 nm,
162 respectively. Firstly, 10 ppm BR18, 10 ml volume and potential (-1.1 V, -1.2 V and -1.3 V)
163 were studied during the 2-hour experiment. Coatings were done at different second (120,180,
164 300 and 420 sec) with the voltage with the best results. Then, the number of electrodes covered
165 (1, 2, 3 and 4 coating), dye concentration (5, 10 and 15 ppm) studies and reuse experiments
166 were carried out. Samples taken from the reactor were measured at 484 nm wavelength using a
167 UV-vis (T90 + UV/VIS Spectrometer, PG Instruments Ltd.) spectrophotometer. The BR18
168 removal efficiency was calculated using the following equation (1).

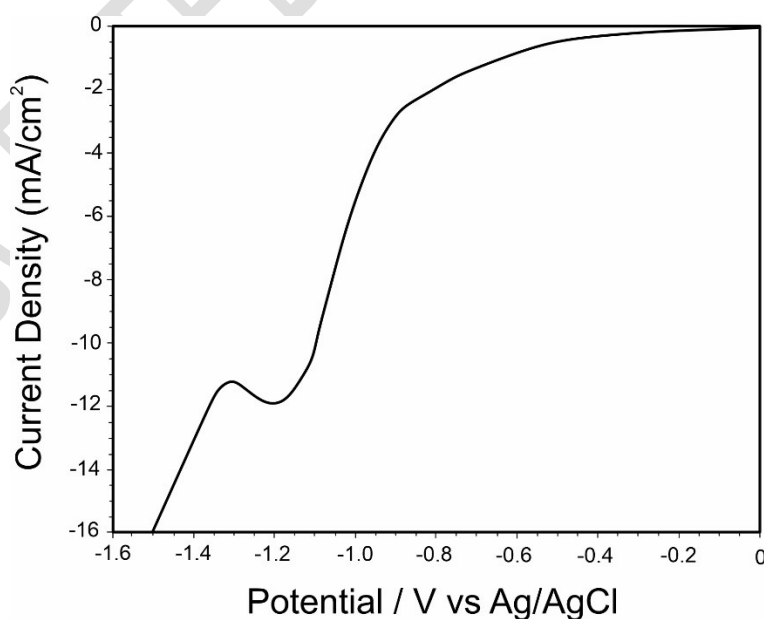
$$169 \quad \text{Removal Efficiency(\%)} = \frac{C_i - C_f}{C_i} * 100 \quad (1)$$

170 where the dye or Cr(VI) concentration at initial (C_i) (mg/L) and the dye or Cr(VI) concentration
171 at final (C_f) (mg/L) are expressed in this particular format.

172 3. Results and Discussion

173 3.1. Effects of electrochemical deposition parameters on ZnO films

174 LSV curve for ZnO films carried out in the potential range 0 to -1.6 V vs Ag/AgCl is shown in
175 Fig. 3.

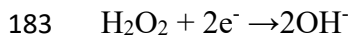


176
177 **Fig. 3.** Linear sweep voltammetry (LSV) curves of the ZnO electrodeposition on a SS electrode
178 from a 0.1 M KCl + 20 mM H₂O₂ + 50 mM ZnCl₂ solution.

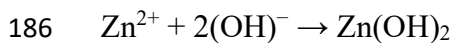
179

180 The ZnO film formation is based the generated OH^- by hydrogen peroxide reduction at the
181 stainless steel interface (Pauporté and Lincot 2001).

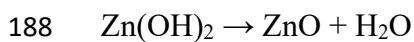
182 First, the reaction that results from the reduction of hydrogen peroxide produces hydroxide ions.



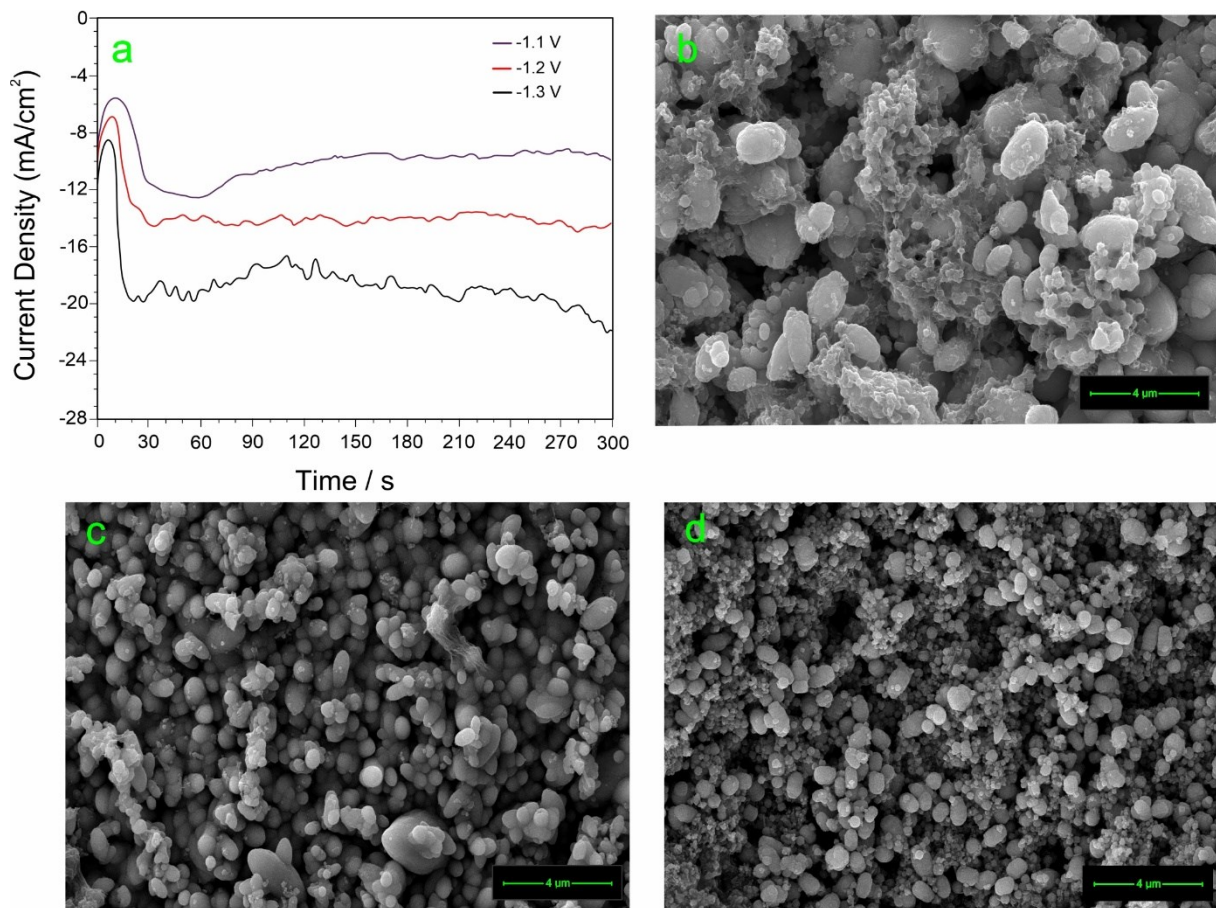
184 Then, the formation of zinc hydroxide takes place by the reaction. The reaction occurs below
185 around -1.1 V.



187 The $\text{Zn}(\text{OH})_2$ dehydrates spontaneously at higher temperature (70 °C) following:

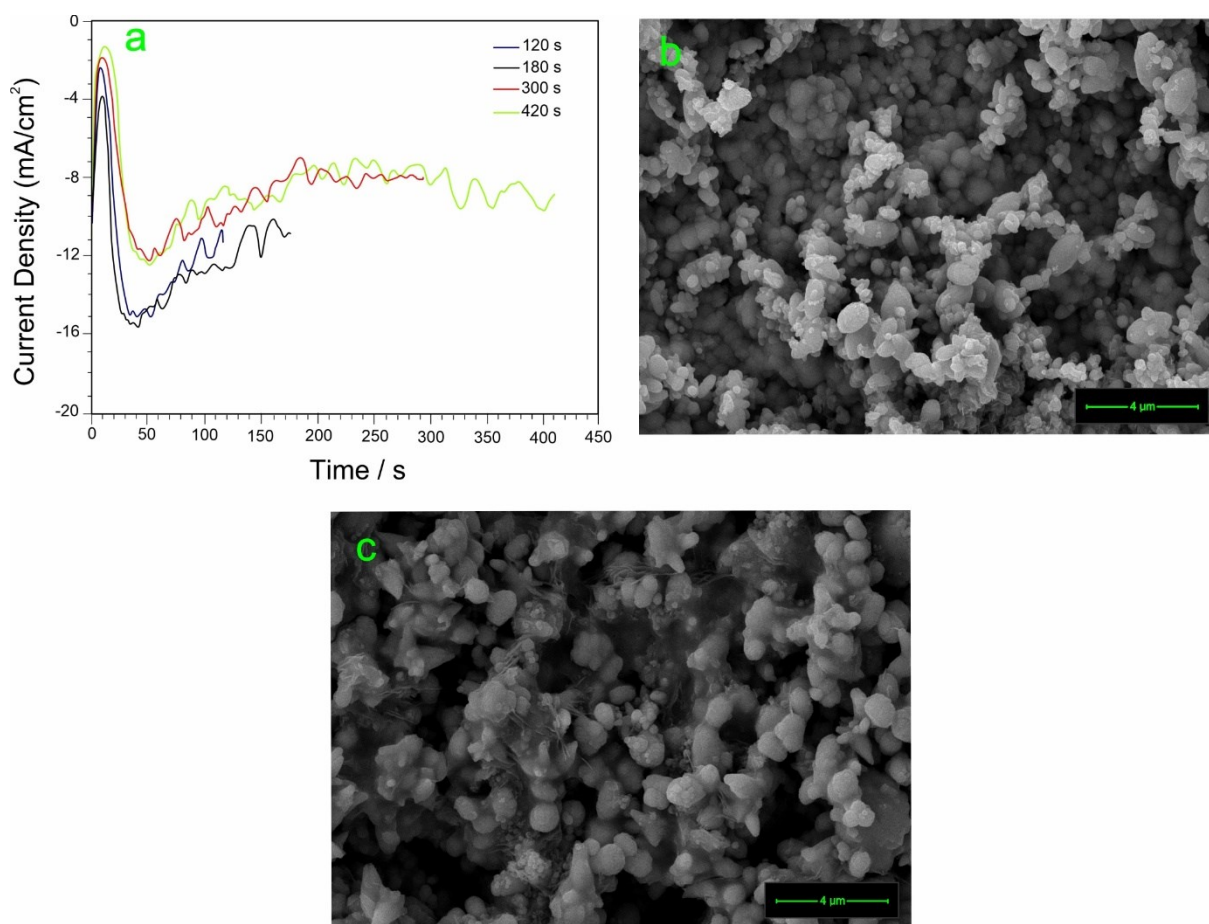


189 Fig. 4a depicts the current density curves after the application of an applied potential from –
190 1.1 to -1.3 V at a constant temperature (70 °C). In order to avoid the formation of H_2 at
191 potentials more negative than -1.3 V, coating processes were not carried out. As expected, it
192 was observed that high current density occurs with the increase of applied cathodic potentials.
193 The cathodic current is directly related to the nucleation rate. As the cathodic current increases,
194 the nucleation steps occur faster. Increasing the nucleation rate supports the presence of high
195 amounts of $\text{Zn}(\text{II})$ ions around the electrode (Patella et al. 2022). This allows ZnO particles to
196 grow vertically on the electrode surface. Figure 4b–d shows the SEM images of ZnO films
197 deposited at potential -1.1 , -1.2 , and -1.3 V, respectively. It can be seen that the type of ZnO
198 seed layers is in the form of nanospheres. Every film exhibits compact and homogeneous
199 deposition. ZnO nanospheres that were deposited at -1.2 V had a mixed morphology, with
200 uniform grains arranged in irregularly shaped clusters and no homogeneous distributions, in
201 contrast to compact, homogeneous, and uniform ZnO nanospheres. For these reasons, the
202 applied potential was determined as -1.2 V to create a good synergistic effect between the
203 density of the ZnO nanospheres and the active surface area.



204
 205 **Fig. 4.** (a) Chronoamperometric curves and SEM images, (b) -1.1 V, (c) -1.2 V and (d) -1.3 V
 206 vs. Ag/AgCl of the ZnO electrodeposition on a SS electrode for 300 s.

207
 208 Fig. 5a shows LSV curves of different ZnO growths on SS surface as a function of the
 209 electrodeposition time. Figure 5b and 4c shows the SEM images of ZnO films deposited at time
 210 120 and 420 s, respectively. It can be observed that two ZnO films appeared of sphere shape
 211 grown perpendicularly on a SS substrate. The SEM images show that amount of ZnO
 212 nanospheres and clustering strongly increases with increasing deposition time. ZnO
 213 nanospheres covered the entire stainless steel surface due to the increased deposition time from
 214 120, 180, 300 and 420 s.

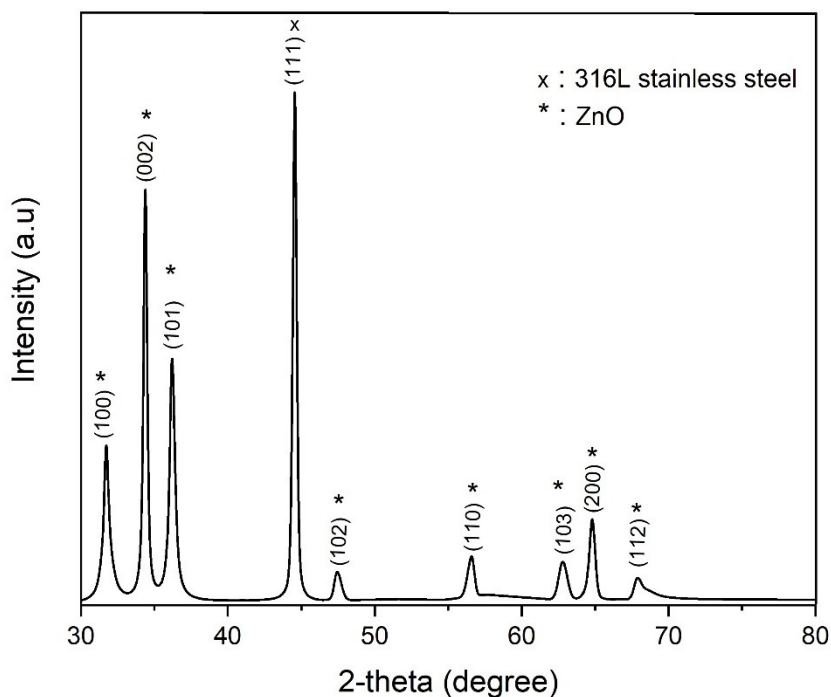


215
 216 **Fig. 5.** (a) Chronoamperometric curves and SEM images, (b) 120 s, and (c) 420 s of the ZnO
 217 electrodeposition on a SS electrode at -1.2 V vs Ag/AgCl.

218
 219 The XRD pattern results of ZnO film is showed in Fig. 6. All the diffraction peaks correspond
 220 to the ZnO wurtzite structure. The diffraction peaks at $2\theta = 31.74^\circ, 34.38^\circ, 36.21^\circ, 47.48^\circ,$
 221 $56.55^\circ, 62.81^\circ, 64.79^\circ$ and 68.05° corresponding to the diffraction planes of (100), (002), (101),
 222 (102), (110), (103), (200) and (112), respectively. This matches the standard values JPDS card
 223 no: 00-36-1451. The Debye-Scherrer formula was used to determine the diameter of the
 224 synthesized ZnO nanoparticle (Shirvani and Naji 2023):

$$d = \frac{K\lambda}{\beta \cos \theta}$$

225
 226 In this case, K is a constant of 0.9, β is the full width at half maximum (FWHM) in radians, λ
 227 is the Bragg angle, and λ is the wavelength of the X-ray (1.5406 Å). A ZnO crystallite size
 228 average of 17.70 nm was determined.



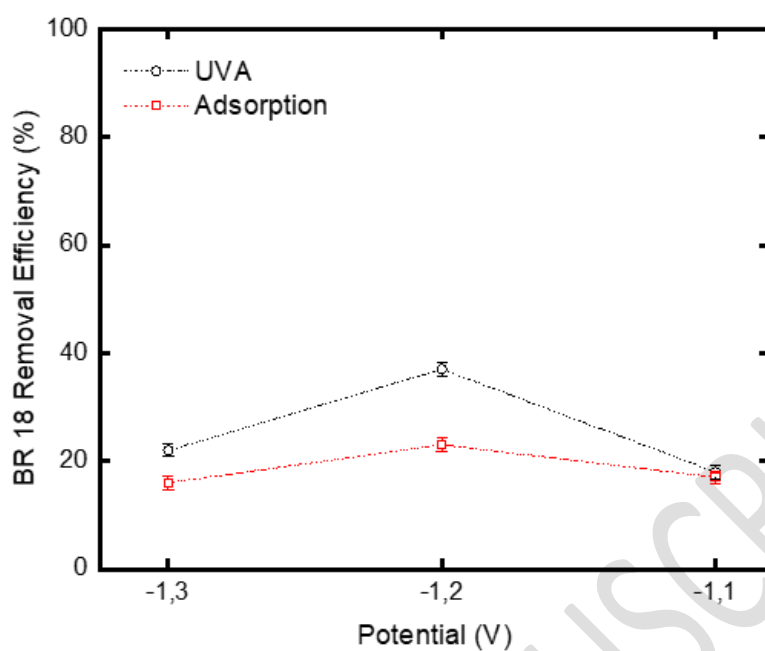
229

230 **Fig. 6.** X-ray diffractograms of ZnO films electrodeposited at -1.2 V vs. Ag/AgCl.

231

232 *3.2. Effect of BR18 removal efficiency at different potentials*

233 Coatings carried out at different potentials from -1.1 to -1.3 V for 180 sec were investigated on
 234 the effect of BR18 dye removal efficiency. Both photocatalytic oxidation and adsorption studies
 235 were carried out under the same conditions. The study was carried out with 10 mg/L BR18 dye
 236 concentration, 2 hours of experimentation and 1 coating (1 cm × 2 cm). The BR18 removal
 237 efficiency graph is given in Figure 7. The coatings made at -1.1 V, -1.2 V and -1.3 V potentials
 238 obtained 18%, 37% and 22% removal efficiency under UVA light, respectively. In the
 239 adsorption study, 17%, 23% and 16% removal efficiencies were achieved.

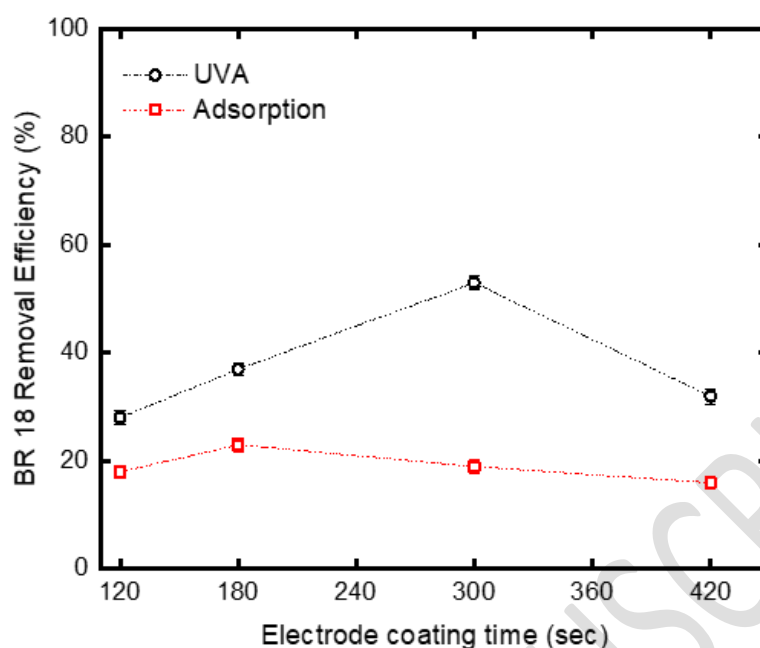


240

241 **Fig. 7.** Effect of different potentials on dye removal efficiency

242 *3.3. The effect of surfaces coated at different times*

243 According to the potential values, the best dye removal efficiency was realized at -1.2 V. For
 244 this reason, further studies were continued with coatings produced at -1.2 V. After the coatings
 245 were made at 120, 180, 300 and 420 seconds, BR18 removal efficiency in UVA and adsorption
 246 was checked for 10 mg/L BR18 dye concentration. The dye removal efficiency graph depending
 247 on the coating time is given in Figure 8. In the photocatalytic study, 28%, 37%, 53% and 32%
 248 removal efficiencies were obtained at 120, 180, 300 and 420 seconds, respectively; 18%, 23%,
 249 19% and 16% removal efficiencies were obtained in the adsorption study. Therefore, 300 sec
 250 coating was chosen for further experiments due to obtaining the highest removal efficiency.



251

252 **Fig. 8.** Effect of different ZnO coating times on dye removal efficiency

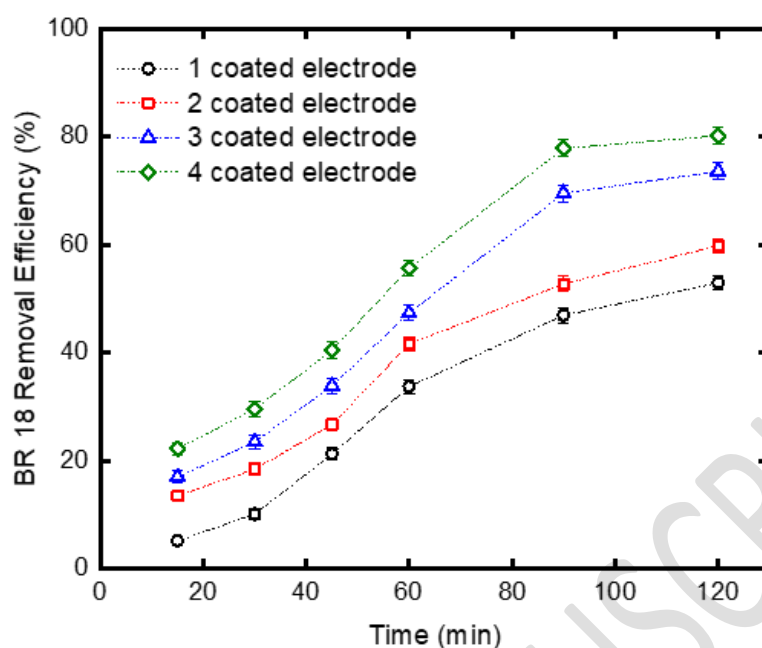
253 *3.4. Effect of coating numbers on dye removal efficiency*

254 The study was continued with the best conditions obtained at -1.2 V and 300 sec coating. The
 255 time dependent dye removal efficiency graph according to the number of coatings is shown in
 256 Figure 9. While 53.0% removal efficiency was obtained in 1 coating, 59.9% removal efficiency
 257 was obtained in 2 coatings, 73.6% in 3 coatings and 80.2% in 4 coatings for 10 mg/L BR18 dye
 258 concentration.

259 In the study conducted by Xu et al. 2020, a sol-gel method was used to deposit Al-doped ZnO
 260 coatings on stainless steel wire mesh. It was observed that the removal efficiency increased as
 261 the amount of ZnO photocatalyst loaded on the stainless steel wire mesh increased. It is
 262 proportional to the higher photocatalytic activity that the ZnO catalyst is covered with more
 263 surface area (Xu et al. 2020).

264 In another study, ZnO aggregations were developed on compacted stainless steel cages and
 265 their photocatalytic effect was examined. It exhibited an improved photocatalytic property
 266 performance compared to the degradation of RhB under UVA light. In the photocatalysis
 267 degradation reaction, when the hierarchical aggregation had larger surface area, it offered more
 268 reaction area due to the larger porous channels in the nanolayers (Li et al. 2016).

269

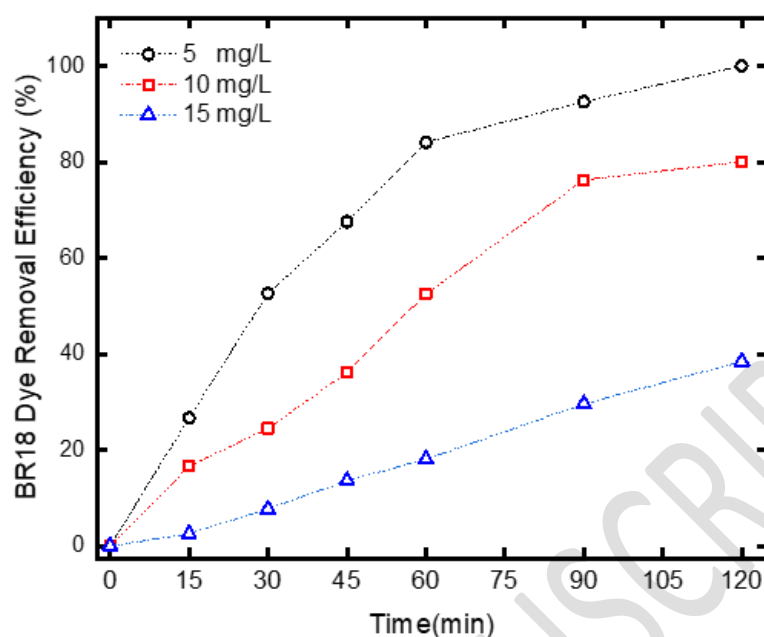


270

271 **Fig. 9.** The effect of the number of coatings on the dye removal efficiency

272 *3.5. Effect of dye concentration*

273 According to previous experiments, optimum conditions were determined as -1.2 V potential,
 274 300 sec coating time and 4 coatings. In these conditions, the time-dependent dye removal
 275 efficiency of 5, 10 and 15 mg/L was investigated. At 5 mg/L, 26% at 15 min and 100% at 120
 276 min were obtained. While it reached from 16% to 80% at 10 ppm, removal efficiency from 2%
 277 to 38% was reached at 15 mg/L. Effect of dye concentration on time-dependent removal
 278 efficiency is given in Figure 10. This decrease is attributed to the decrease in light absorption
 279 on the catalyst surface with increasing dye concentration. In addition, photo-elimination is
 280 associated with insufficient OH radical formation. Shubha et al. 2023 investigated the
 281 photocatalytic degradation of textile dyes with nickel oxide (NiO-SD) NPs. Malachite green
 282 (MG) and methylene blue (MB) were used in the study. The dye concentration was tested as
 283 4.8, 12 and 16 ppm. It was observed that the removal efficiency of both dyes decreased
 284 significantly as the dye concentration increased (Shubha et al. 2023).



285

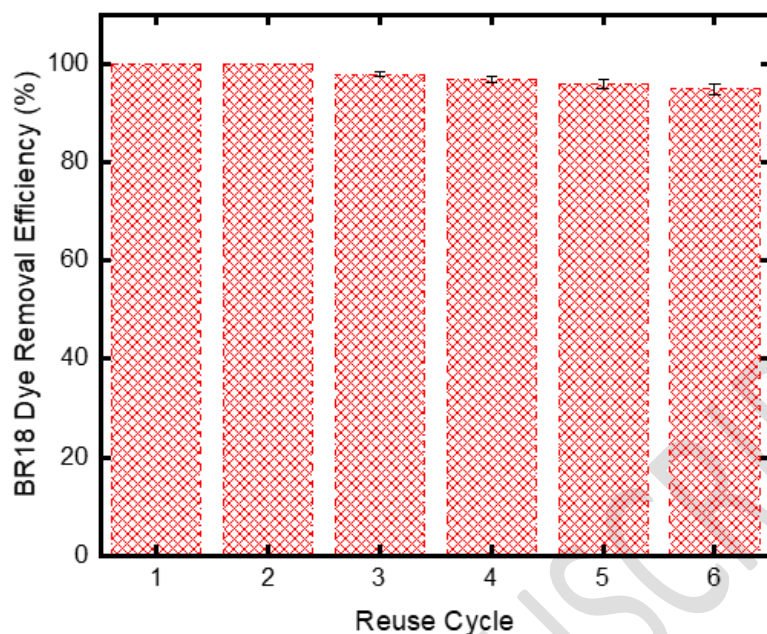
286 **Fig. 10.** Effect of dye concentration on time-dependent removal efficiency

287 *3.6. Reuse cycle*

288 The reuse of the synthesized material under optimum conditions was studied. In previous
 289 studies, optimum conditions were determined as 5 ppm BR18 concentration, 4 coatings, 300
 290 sec coating time and -1.2 V potential. After the coating was washed with distilled water after
 291 each use, dye was added and reuse studies were continued. The reuse graph is given in Figure
 292 11. While 100% removal efficiency was obtained in the 1st and 2nd reuses, 95% removal
 293 efficiency were obtained after 5th subsequent uses. Xu et al. 2020 was used for photocatalytic
 294 degradation of MB several times under the same operating conditions. After four times of
 295 photocatalytic reaction, it was observed that the degradation efficiency of the catalyst was not
 296 greatly reduced, thus the catalyst exhibited a good condition in terms of reusability. The slight
 297 decrease in the photocatalytic activity of the catalyst is explained as the changes in the surface
 298 modification due to the photocorrosion of ZnO (Xu et al. 2020).

299 In another study, photodegradation of RhB was observed over ten cycles. After each cycle, the
 300 catalyst was washed several times using deionized water and fresh RhB solution was added.
 301 The constant photodegradation rate over ten consecutive cycles showed that the catalyst was
 302 stable under different light intensity (Li et al. 2016).

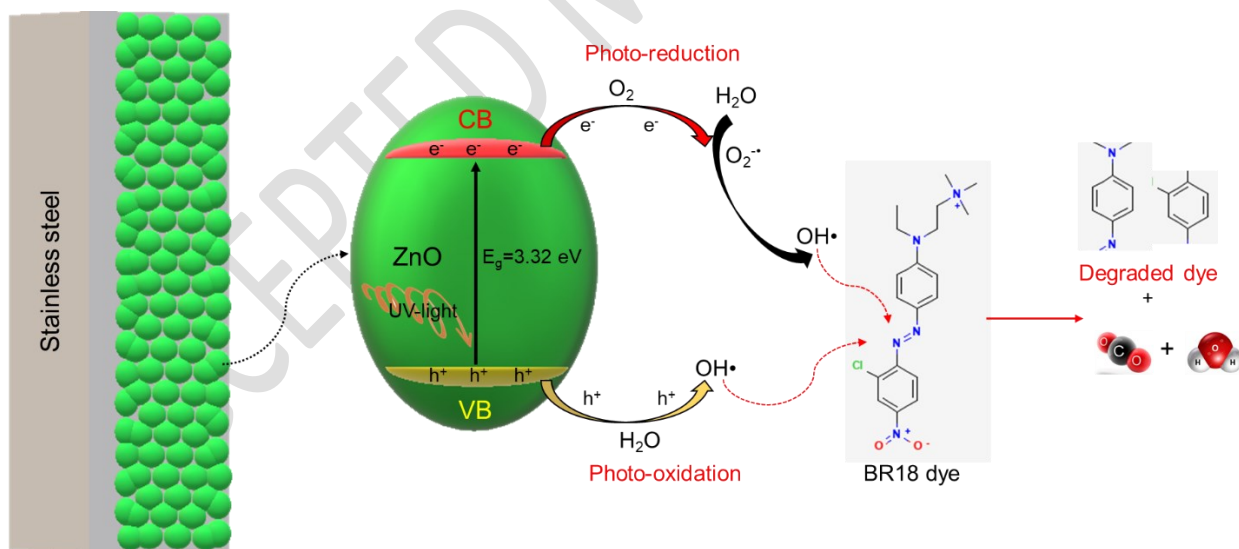
303



304

305 **Fig. 11.** Reuse cycle of BR 18 dye photo-degradation

306 The proposed photo degradation mechanism of BR 18 dye using electrochemically deposited
 307 zinc oxide films on stainless steel are illustrated in Scheme 1.



308

309 **Scheme 1.** Schematic illustrations for photocatalytic degradation mechanism of BR18 dye

310 4. Conclusion

311 In this study, ZnO films were successfully deposited onto on a stainless steel by electrochemical
 312 method. The effect of ZnO films on dye removal by photocatalytic oxidation was investigated.
 313 Deposition parameters such as deposition time and deposition potential in electroplating are

314 optimized for the preparation of ZnO films with the largest surface area, particle distribution
315 and good catalytic effect for dye removal efficiency.

316 Potentially the best dye removal efficiency was also obtained, while the best removal efficiency
317 was obtained at 300 second in time. The BR18 removal efficiency was achieved by performing
318 the number of electrodes covered (1, 2, 3 and 4 coating) and dye concentration (5, 10 and 15
319 mg/L) tests with the coating obtained at the best potential and time. For 10 mg/L BR18
320 concentration, 53% removal efficiency was obtained in 1 coating, while it increased to 80.2%
321 in 4 coatings. In dye concentration, 100%, 80% and 38.5% removal efficiency was obtained at
322 5, 10 and 15 mg/L, respectively, by using 4 electrode coatings. With -1.2 V potential, 300 sec
323 coating time, 4 coated electrodes and 5 mg/L dye concentration, 100% removal efficiency was
324 achieved and reuse studies were carried out under these conditions. It was reused 5 times and
325 100% removal efficiency was achieved in the first 2 uses. In subsequent use, removal efficiency
326 decreased to 95% after 5th repeated use.

327 **References**

328 Antoniadis, A., Takavakoglou, V., Zalidis, G., Poullos, I., (2007). "Development and evaluation
329 of an alternative method for municipal wastewater treatment using homogeneous photocatalysis
330 and constructed wetlands." Catalysis Today **124**(3): 260-265.

331
332 Bethi, B., Sonawane, S.H. Bhanvase, B.A. Gumfekar, S.P., (2016). "Nanomaterials-based
333 advanced oxidation processes for wastewater treatment: A review." Chemical Engineering and
334 Processing - Process Intensification **109**: 178-189.

335
336 Earnhart, D. (2013). Water Pollution from Industrial Sources. Encyclopedia of Energy, Natural
337 Resource, and Environmental Economics. J. F. Shogren. Waltham, Elsevier: 114-120.

338
339 Elshahawy, M. F., Abd A.N., Mohamed, R.D., El-Hag A.A. (2023). "Radiation synthesis and
340 photocatalytic performance of floated graphene oxide decorated ZnO/ alginate-based beads for
341 methylene blue degradation under visible light irradiation." International Journal of Biological
342 Macromolecules **243**: 125121.

343 Eskikaya, O., Ozdemir, S., Tollu, G., Dizge, N., Ramaraj, R., Manivannan, A., Balakrishnan,
344 D., (2022). "Synthesis of two different zinc oxide nanoflowers and comparison of antioxidant
345 and photocatalytic activity." Chemosphere, **306**: 135389.

346
347 Fiorenza, R., Spitaleri, L., Perricelli, F., Nicotra, G., Fragalà, M.E., Scirè, S., Gulino, A. (2023).
348 "Efficient photocatalytic oxidation of VOCs using ZnO@Au nanoparticles." Journal of
349 Photochemistry and Photobiology A: Chemistry **434**: 114232.

350

351 Ghalebizade, M. and B. Ayati (2016). "Solar photoelectrocatalytic degradation of Acid Orange
352 7 with ZnO/TiO₂ nanocomposite coated on stainless steel electrode." Process Safety and
353 Environmental Protection **103**: 192-202.

354
355 Hasanbeigi, A. and L. Price (2015). "A technical review of emerging technologies for energy
356 and water efficiency and pollution reduction in the textile industry." Journal of Cleaner
357 Production **95**: 30-44.

358
359 Kohzadi, S., Maleki, A., Bundschuh, M., Vahabzadeh, Z., Johari, S.A., Rezaee, R., Shahmoradi,
360 B., Marzban, N., Amini, N. (2023). "Doping zinc oxide (ZnO) nanoparticles with molybdenum
361 boosts photocatalytic degradation of Rhodamine b (RhB): Particle characterization, degradation
362 kinetics and aquatic toxicity testing." Journal of Molecular Liquids **385**: 122412.

363
364 Kumar, S., Kaushik, R.D., Purohite, L.P. (2021). "Novel ZnO tetrapod-reduced graphene oxide
365 nanocomposites for enhanced photocatalytic degradation of phenolic compounds and MB dye."
366 Journal of Molecular Liquids **327**: 114814.

367
368 Lamkhao, S., Tandorn, S., Rujijanagul, G., Randorn, C., (2023). "A practical approach using a
369 novel porous photocatalyst/hydrogel composite for wastewater treatment." Materials Today
370 Sustainability: 100482.

371
372 Li, Z., Liu, G., Zhang, Y., Zhou, Y., Yang, Y. (2016). "Porous nanosheet-based hierarchical
373 zinc oxide aggregations grown on compacted stainless steel meshes: Enhanced flexible dye-
374 sensitized solar cells and photocatalytic activity." Materials Research Bulletin **80**: 191-199.

375
376 Rekha, S.M., Neelamana, H.V., Bhat, S. V. (2023). "Recent Advances in Solution-Processed
377 Zinc Oxide Thin Films for Ultraviolet Photodetectors." ACS Applied Electronic Materials **5**(8):
378 4051-4066.

379 Mahmoodi, N.M., Hosseinabadi-Farahani, Z., Chamani, H., (2016). "Synthesis of
380 nanostructured adsorbent and dye adsorption modeling by an intelligent model for
381 multicomponent systems." Korean J. Chem. Eng., **33**(3), 902-913.

382
383 Naseri, A., Samadi, M., Pourjavadi, A., Ramakrishna, S., Moshfegh, A.Z, (2021). "Enhanced
384 photocatalytic activity of ZnO/g-C₃N₄ nanofibers constituting carbonaceous species under
385 simulated sunlight for organic dye removal." Ceramics International **47**(18): 26185-26196.

386
387 Patella, B., Moukri, N., Regalbuto, G., Cipollina, C., Pace, E., Di Vincenzo, S., Aiello, G.,
388 O'Riordan, A., Inguanta, R. (2022). "Electrochemical Synthesis of Zinc Oxide Nanostructures
389 on Flexible Substrate and Application as an Electrochemical Immunoglobulin-G
390 Immunosensor." Materials **15**(3): 713.

391
392 Pauporté, T. and D. Lincot (2001). "Hydrogen peroxide oxygen precursor for zinc oxide
393 electrodeposition II—Mechanistic aspects." Journal of Electroanalytical Chemistry **517**(1): 54-
394 62.

395
396 Roy, M., Sen, P., Pal, P., (2020). "An integrated green management model to improve
397 environmental performance of textile industry towards sustainability." Journal of Cleaner
398 Production **271**: 122656.

399 Saleh, M., Bilici, Z., Kaya, M., Yalvac, M., Arslan, H., Yatmaz, H.C., Dizge, N., (2021). "The
400 use of basalt powder as a natural heterogeneous catalyst in the Fenton and Photo-Fenton
401 oxidation of cationic dyes." Advanced Powder Technology, **32**(4): 1264-1275.

402
403 Selvaraj, S., Patrick S.D, Vangari, G.A. Mohan, M. K., Ponnusamy S, Muthamizchelvan C.
404 (2022). "Facile synthesis of Sm doped ZnO nanoflowers by Co-precipitation method for
405 enhanced photocatalytic degradation of MB dye under sunlight irradiation." Ceramics
406 International **48**(19, Part B): 29049-29058.

407
408 Shirvani, M. and L. Naji (2023). "Comparative study on the electrochemical synthesis of zinc
409 oxide nanorods using chronoamperometry and chronopotentiometry and their application in
410 inverted polymer solar cells." Colloids and Surfaces A: Physicochemical and Engineering
411 Aspects **660**: 130889.

412
413 Shubha, J. P., Savitha, H.S., Patil, R.C., Assal, M.E., Shaik, M.R., Kuniyil, M., Alduhaish, O.,
414 Dubasi, N., Adil, S.F. (2023). "A green approach for the degradation of toxic textile dyes by
415 nickel oxide (NiO-SD) NPs: Photocatalytic and kinetic approach." Journal of King Saud
416 University - Science **35**(7): 102784.

417
418 Singh, S. (2022). "Natural sunlight driven photocatalytic performance of Ag/ZnO
419 nanocrystals." Materials Today Communications **33**: 104438.

420
421 Tao, P. and Y. Wang (2023). "Enhanced photocatalytic performance of W-doped TiO₂
422 nanoparticles for treatment of Procion Red MX-5B azo dye in textile wastewater." International
423 Journal of Electrochemical Science **18**(9): 100261.

424
425 Tarazona, J. V. (2014). Pollution, Water. Encyclopedia of Toxicology (Third Edition). P.
426 Wexler. Oxford, Academic Press: 1024-1027.

427
428 Ugur, N. Bilici, Z. Ocakoglu, K. Dizge, N. (2021). "Synthesis and characterization of composite
429 catalysts comprised of ZnO/MoS₂/rGO for photocatalytic decolorization of BR 18 dye." Colloids and Surfaces A: Physicochemical and Engineering Aspects, **626**: 126945.

430
431 Xu, L., Xian, F., Pei, S., Zhu, Y.. (2020). "Photocatalytic degradation of organic dyes using
432 ZnO nanorods supported by stainless steel wire mesh deposited by one-step method." Optik
433 **203**: 164036.